Electronic Supplementary Information

Experimental section

Materials: Bismuth trichloride ($BiCl_3$), concentrated hydrochloric acid (HCl), ammonium chloride (NH_4Cl), salicylic acid ($C_7H_6O_3$), sodium citrate dehydrate ($C_6H_5Na_3O_7 \cdot 2H_2O$), sodium nitroferricyanide dihydrate ($C_5FeN_6Na_2O \cdot 2H_2O$), sodium hypochlorite solution (NaClO) and Nafion (5wt%) sodium were purchased from Aladdin Ltd. in Shanghai. Para-(dimethylamino) benzaldehyde ($C_9H_{11}NO$), hydrazine hydrate ($N_2H_4 \cdot H_2O$), sodium hydroxide (NaOH), hydrochloric acid (HCl), ethanol (CH_3CH_2OH), Bi foil and carbon paper were bought from Beijing Chemical Corporation. The ultrapure water were purified through a Millipore system used throughout all experiments.

Preparation of Bi NS/CF: Bi nanosheet array was prepared through electrodeposition on CF. In a typical synthesis process, an aqueous solution was obtained by mixing 0.63 g $BiCl_3$, 1.44 mL HCl and 60 mL water. Pulse current electrodeposition was conducted in a standard three electrode system with a working electrode of Cu plate, an Ag/AgCl reference electrode and a platinum counter electrode. Deposition of Bi was carried out potentiostatically at –0.1 V vs. Ag/AgCl for 1 min at room temperature (pulse deposition for 6 cycles with 10 s pulse-on and 40 s pulse-off one cycle) and then the sample was rinsed with water for several times.

Characterization: XRD data were obtained from a LabX XRD-6100 X-ray diffractometer with Cu Kα radiation (40 kV, 30 mA) of wavelength 0.154 nm (SHIMADZU, Japan). SEM images were collected using the tungsten lamp-equipped SU3500 scanning electron microscope at an accelerating voltage of 20 kV (Hitachi, Japan). The structures of the samples were determined by TEM images on a HITACHI H-8100 electron microscopy (Hitachi, Tokyo, Japan) operated at 200 kV. The absorbance data of spectrophotometer were measured on SHIMADZU UV-2700 UV-Vis spectrophotometer. The N_2 temperature-programmed desorption (N_2-TPD) spectrum was tested by using TP-5076 TPD experimental device. Ion chromatograph (IC) data were acquired on Thermofisher ICS 5000 plus ion chromatography,

contained dual temperature heater, injection valve, conductivity detector, AERS 500 Anions suppressor. ^{1}H nuclear magnetic resonance spectra (NMR) were collected on a superconducting-magnet NMR spectrometer (Bruker AVANCE III HD 500 MHz) and dimethyl sulphoxide was used as an internal to calibrate the chemical shifts in the spectra.

Electrochemical measurement: Electrochemical NRR measurements were performed in a two-compartment cell separated by a proton exchange membrane using a CHI 660E electrochemical analyzer (CH Instruments, Inc.). The electrochemical experiments were carried out with a three-electrode configuration using graphite plate as the counter electrode and Ag/AgCl/saturated KCl as the reference electrode. A Bi NS/CF electrode with area of 1 x 1 cm^2 was used as working electrode. The potentials reported in this work were converted to reversible hydrogen electrode (RHE) scale via calibration with the following equation: E (vs. RHE) = E (vs. Ag/AgCl) + 0.197 + 0.059 × pH (V). HCl electrolyte was purged with N_2 for 30 min before the measurement.

Determination of NH_3: 2 mL electrolyte was taken from the cathodic chamber, and then 2 mL of 1 M NaOH solution containing 5% $C_7H_6O_3$ and 5% $C_6H_5Na_3O_7{\cdot}2H_2O$ was added into this solution. Subsequently, 1 mL of 0.05 M NaClO and 0.2 mL of 1% $C_5FeN_6Na_2O{\cdot}2H_2O$ were add into the above solution. After standing at room temperature for 2 h, the UV-Vis absorption spectrum was measured at a wavelength of 658.8 nm. The concentration-absorbance curves were calibrated using standard NH_3 solution with a series of concentrations. The fitting curve ($y = 0.390x + 0.043$, $R^2 = 0.999$) shows good linear relation of absorbance value with NH_3 concentration by three times independent calibrations.

Determination of FE: The FE for N_2 reduction was defined as the amount of electric charge used for synthesizing NH_3 divided the total charge passed through the electrodes during the electrolysis. The total amount of NH_3 produced was measured using colorimetric methods. Assuming three electrons were needed to produce one NH_3 molecule, the FE could be calculated as follows: $FE = (3F \times c_{NH3} \times V)/(17 \times Q)$, where c_{NH3} is the measured NH_3 concentration, V is the volume of electrolyte, F is the

Faraday constant and Q is the quantity of applied electricity. The rate of NH_3 formation was firstly calculated using the following equation: $v_{NH3} = (c_{NH3} \times V)/(17 \times t \times A)$, where t is the reduction reaction time and A is the effective area of the cathode. *Determination of N_2H_4*: A mixed solution of 5.99 g $C_9H_{11}NO$, 30 mL concentrated HCl and 300 mL ethanol was used as a color reagent. Calibration curve was plotted as follow: firstly, preparing a series of reference solutions (10 mL); secondly, adding 5 mL above prepared color reagent and stirring 20 min at room temperature; finally, the absorbance of the resulting solution was measured at 455 nm, and the yields of N_2H_4 were estimated from a standard curve using 5 mL residual electrolyte and 5 mL color reagent. Absolute calibration of this method was achieved using $N_2H_4 \cdot H_2O$ solutions of known concentration as standards, and the fitting curve shows good linear relation of absorbance with $N_2H_4 \cdot H_2O$ concentration ($y = 0.706x + 0.033$, $R^2 = 0.999$) by three times independent calibrations.

Details of DFT calculations: First-principles calculations were performed using the Vienna Ab initio Simulation Package (VASP)[1–3] to investigate the N_2 fixation on the rhombohedral Bi (012) surface. The valence-core electron interactions were treated by Projector Augmented Wave (PAW)[4] methods and the electron exchange correlation interactions were described by the generalized gradient approximation (GGA) with the Perdew-Burke-Emzerhof (PBE)[5] functional. Van der Waals interactions were considered using DFT-D3 with Becke-Jonson damping method. The surface model was constructed with a 2×2×1 supercell containing 6 atom-layer slab, and a 15 Å vacuum along the z direction. The energy cutoff was set to 450 eV and the convergent criterion of geometry relaxation was set as the force on each atom is less than 0.02 eV/Å. The K points in the Brillouin zone were sampled with 3×3×1 by the Monkhorst-Pack[6] scheme. The free energy changes of the NRR steps were calculated by the equation:[7] $\Delta G = \Delta E_{DFT} + \Delta E_{ZPE} - T\Delta S$, where ΔE_{DFT} is the DFT obtained binding energy, ΔE_{ZPE} is the difference in zero-point energy correction, ΔS is entropy change calculated by vibration analysis, and T is the temperature set to 300 K. The free energy corrections of NH_3, H_2 and N_2 molecules were taken from the database. (Computational Chemistry Comparison and Benchmark Database.

http://cccbdb.nis.gov/.).

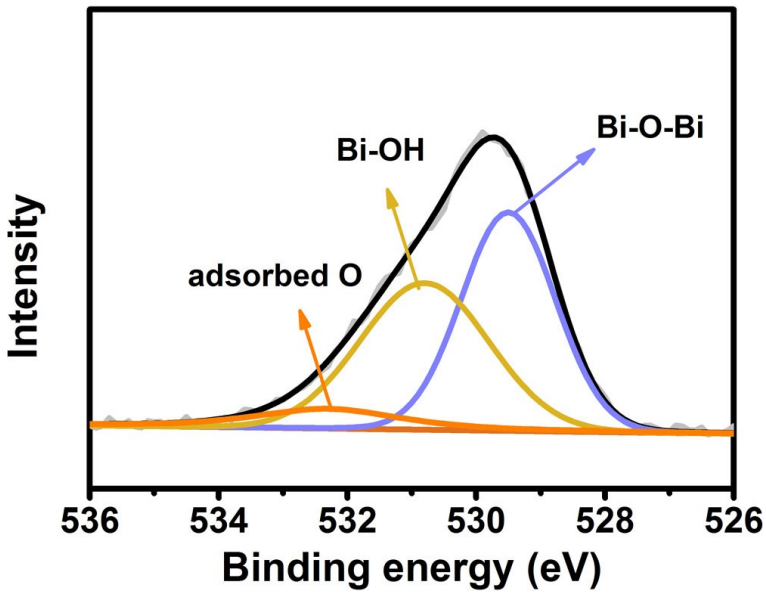

Fig. S1. XPS spectrum in the O 1s region of Bi catalyst.

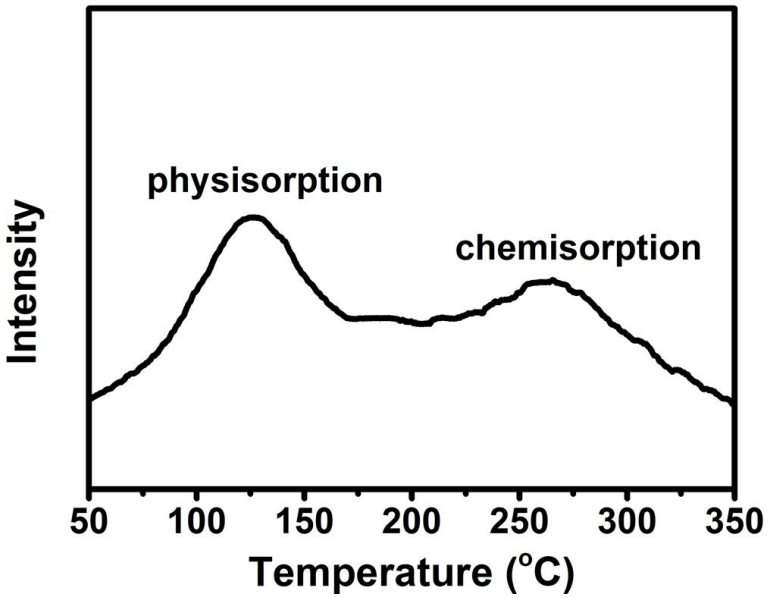

Fig. S2. N_2-TPD curve of Bi.

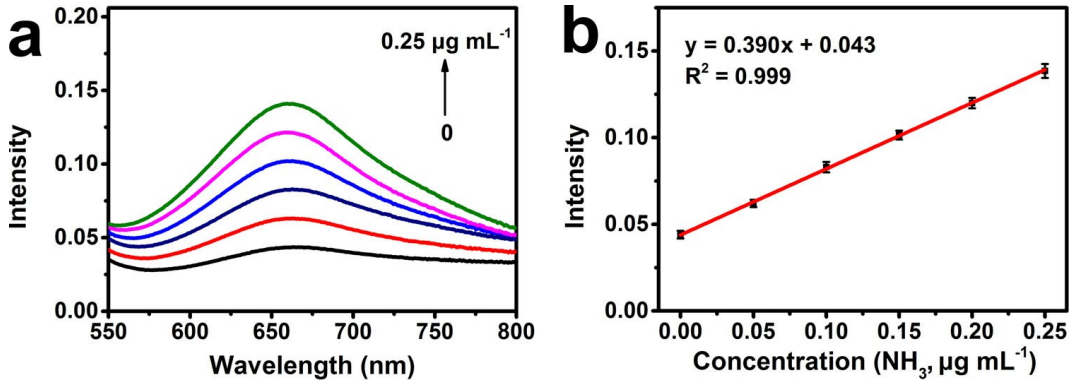

Fig. S3. UV-Vis absorption curves of various concentrations of NH_3 stained with indophenol indicator and incubated for 2 h at room temperature. (b) Calibration curve used to estimate the concentrations of NH_3.

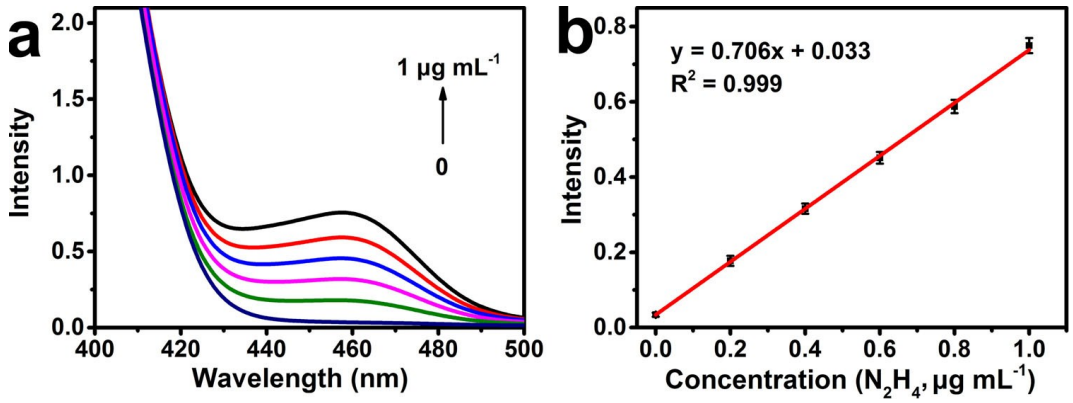

Fig. S4. (a) UV-Vis curves of various concentrations of N_2H_4 stained with *p*-$C_9H_{11}NO$ indicator and incubated for 20 min at room temperature. (b) Calibration curve used to calculate the concentrations of N_2H_4.

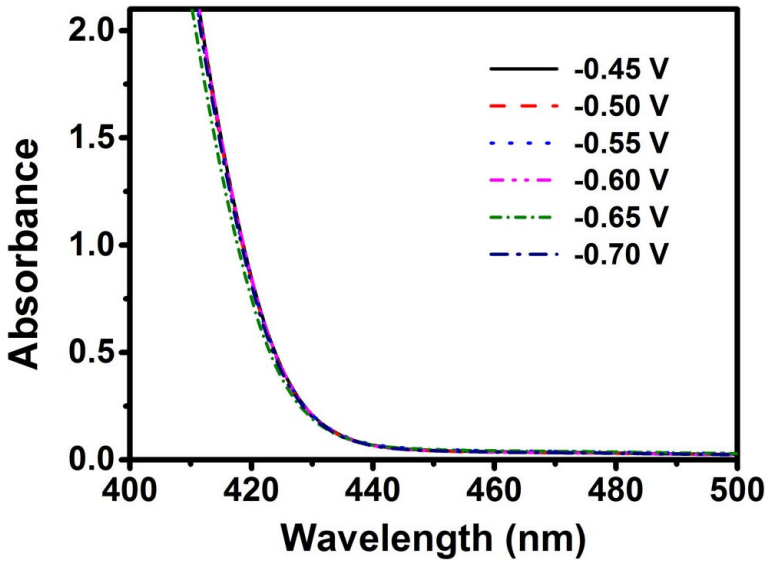

Fig. S5. UV-Vis absorption spectra of the electrolytes stained with *p*-$C_9H_{11}NO$ indicator after 2-h electrolysis using Bi NS/CF at a series of potentials.

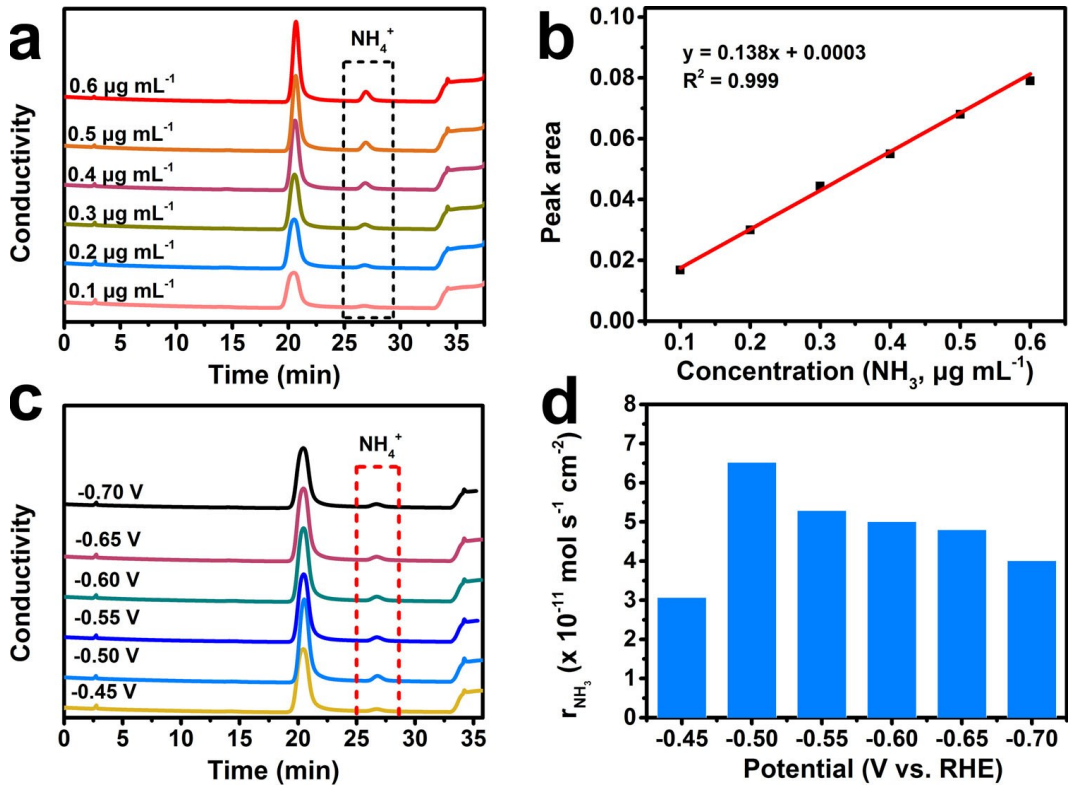

Fig. S6. (a) IC data for different concentrations of NH_4^+. (b) Calibration curve obtained from IC. (c) IC data for the electrolytes at different potentials after 4-h electrolysis using Bi NS/CF. (d) NH_3 yield rates of Bi NS/CF at different potentials obtained from IC.

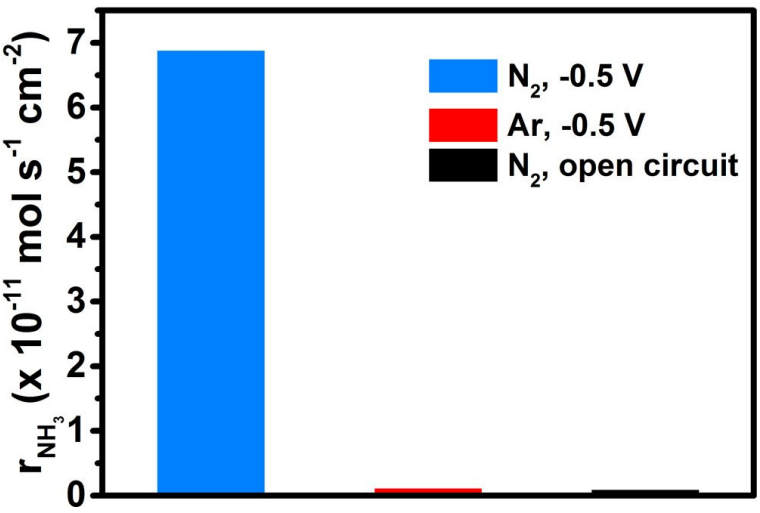

Fig. S7. NH_3 yields under different conditions using Bi NS/CF.

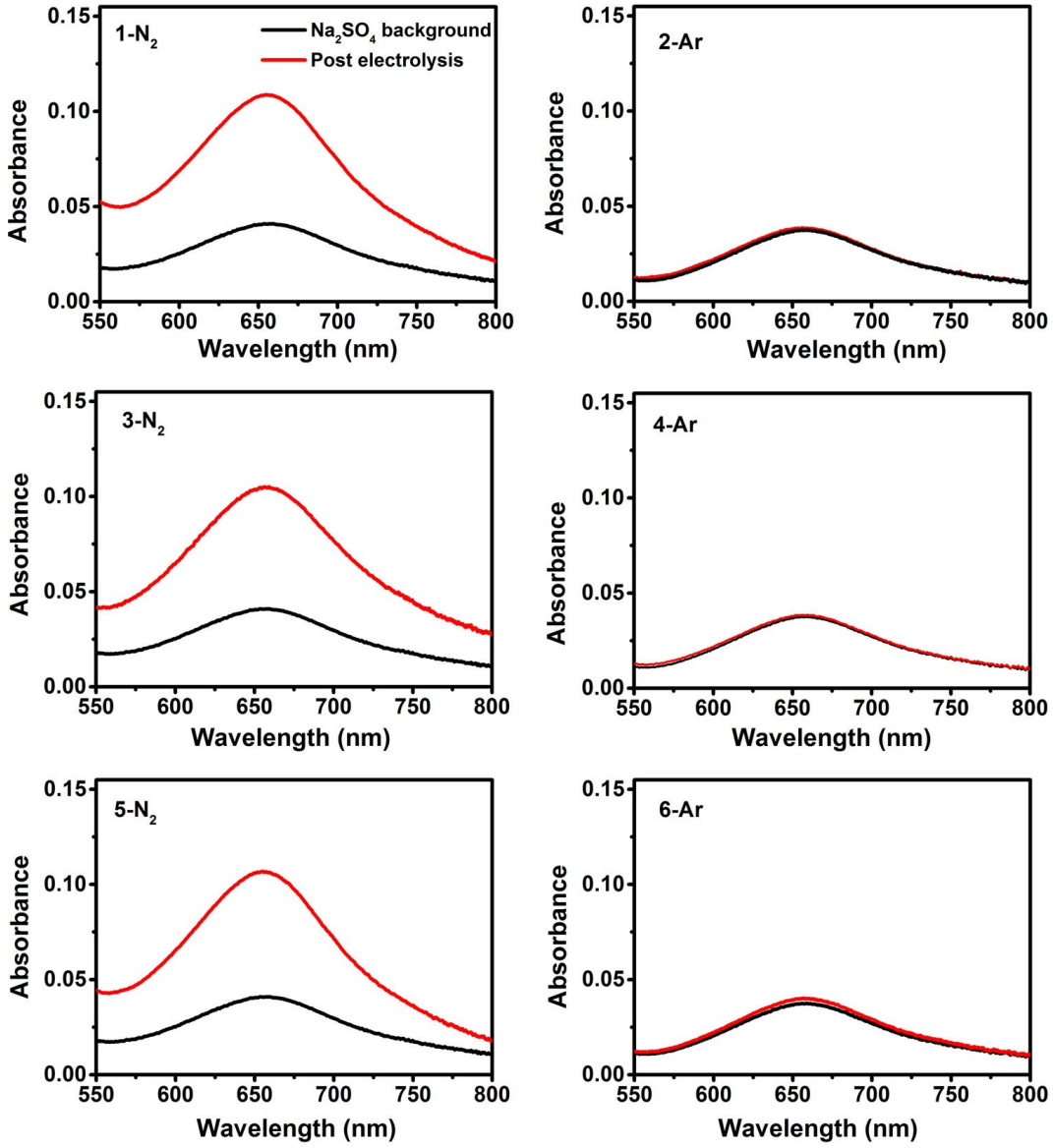

Fig. S8. Control experiments results by alternately flowing N_2 and Ar gas into the electrolytes to verify the production of NH_3, which were repeated three times consecutively.

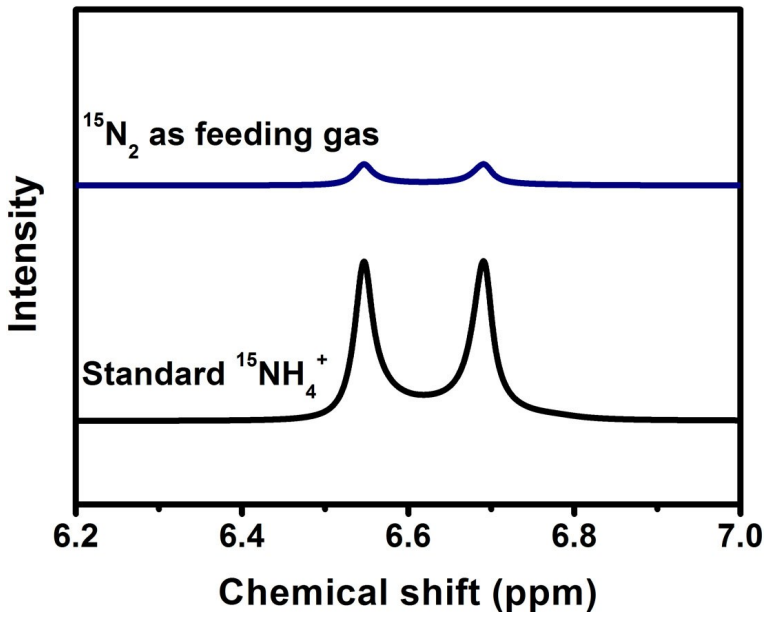

Fig. S9. The ^{1}H NMR spectra for $^{15}NH_4^+$ standard sample and the product using $^{15}N_2$ as the feeding gas.

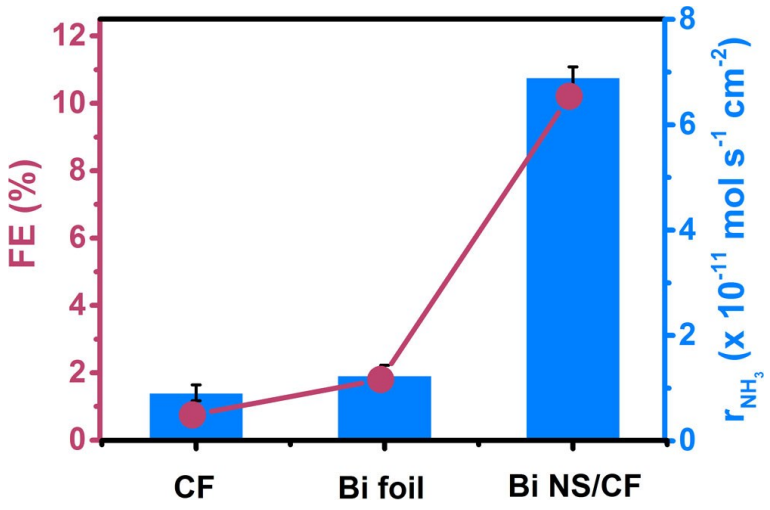

Fig. S10. NH_3 yield rates and FEs of CF, Bi foil and Bi NS/CF at –0.50 V.

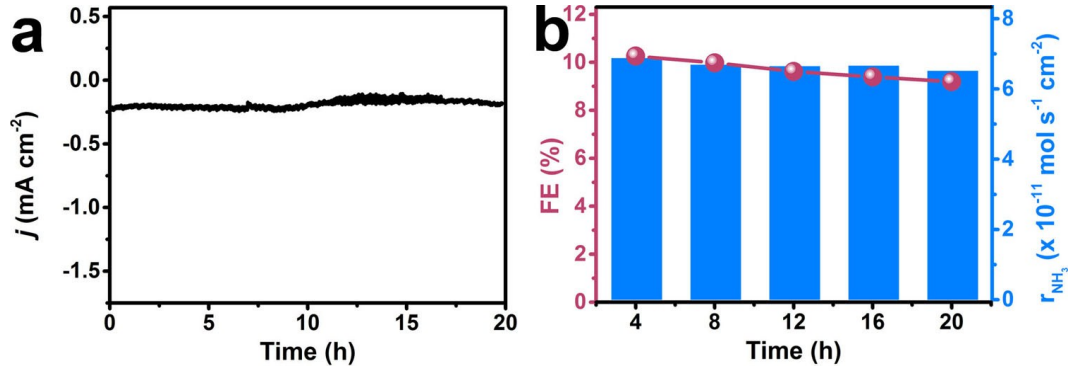

Fig. S11. (a) Long-term electrochemical stability test of Bi NS/CF at –0.50 V for 20 h. (b) NH_3 yield rates and FEs of Bi NS/CF during 24-h stability test.

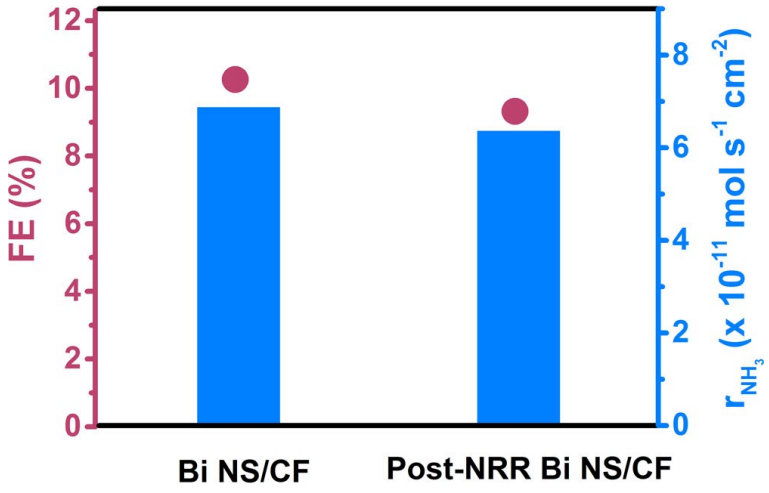

Fig. S12. NH_3 yield rates and FEs of Bi NS/CF before and after 24-h stability test at –0.50 V.

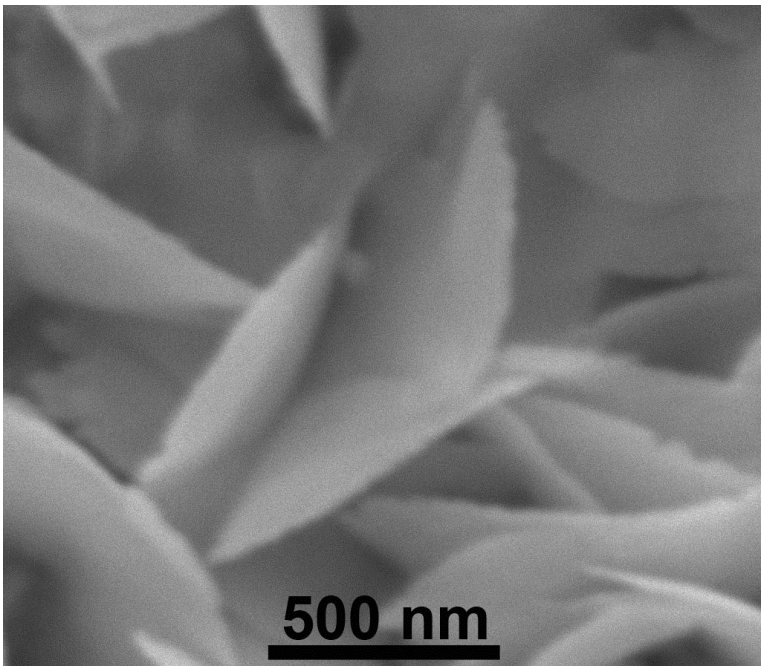

Fig. S13. SEM image of Bi NS/CF after stability test.

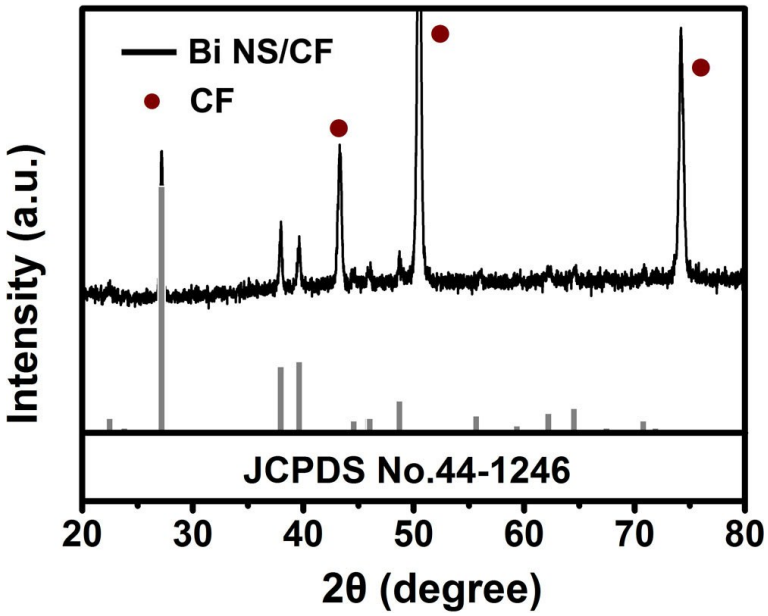

Fig. S14. XRD pattern of Bi NS/CF after stability test.

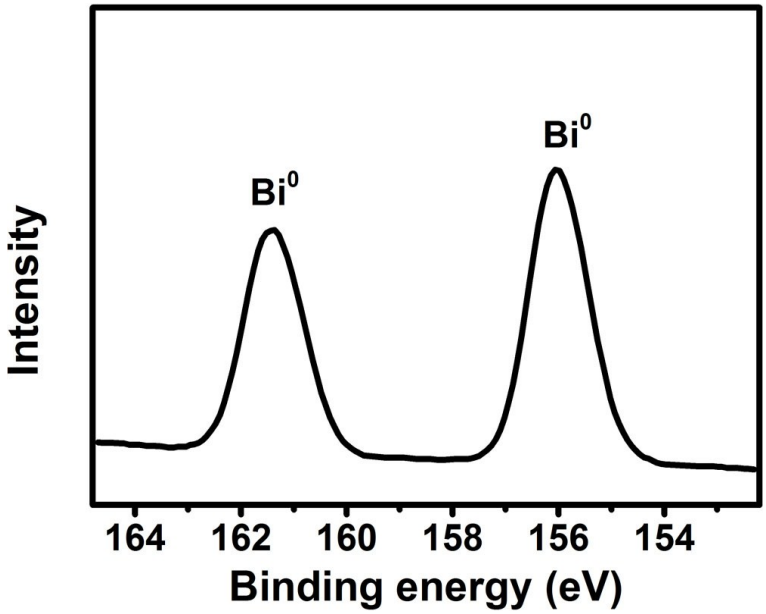

Fig. S15. XPS spectrum in the Bi 4f region of post-NRR Bi catalyst.

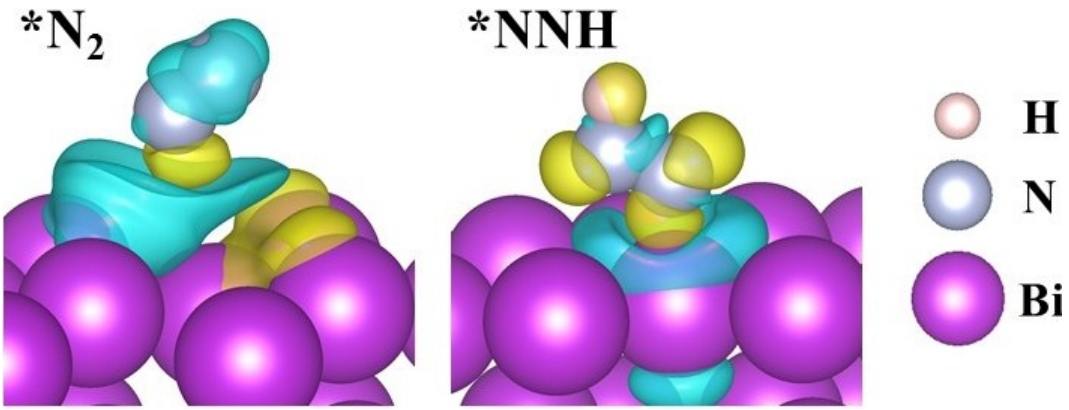

Fig. S16. Charge density difference of the *N_2 and *NNH states.

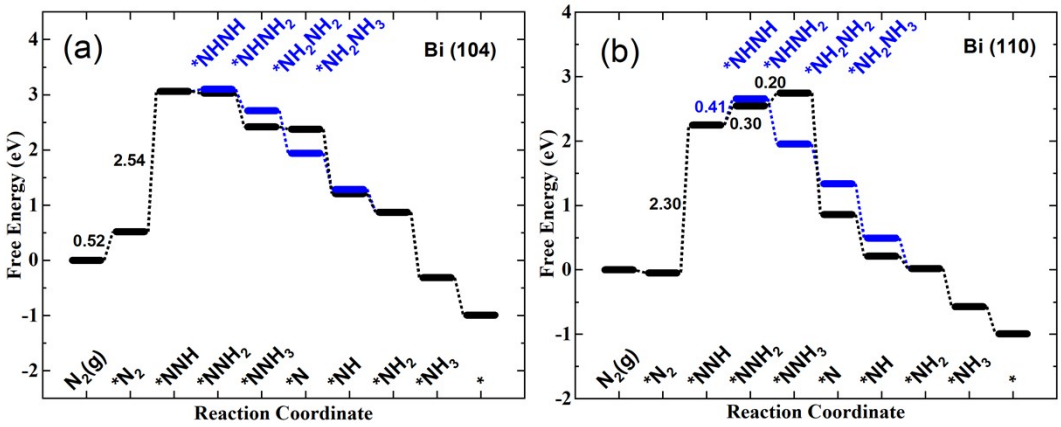

Fig. S17. Free energy profile of NRR process on (a) Bi (104) and (b) Bi (110). An asterisk (*) denotes as the adsorption site.

Table S1. Comparison of NH_3 yield rate and FE of Bi NS/CF to produce NH_3 with other reported NRR electrocatalysts in acids under ambient conditions.

Catalyst	Electrolyte	NH_3 yield rate	FE (%)	Ref.
Bi NS/CF	0.1 M HCl	6.89×10^{-11} mol s^{-1} cm^{-2}	10.26	This work
		4.21 μg h^{-1} cm^{-2}		
		5.26 μg h^{-1} $mg^{-1}_{cat.}$		
Black phosphorus sheets	0.01 M HCl	31.37 μg h^{-1} $mg^{-1}_{cat.}$	5.07	8
Boron-doped graphene	0.05 M H_2SO_4	9.8 μg h^{-1} cm^{-2}	10.8	9
N-doped porous carbon	0.05 M H_2SO_4	23.8 μg h^{-1} $mg^{-1}_{cat.}$	1.42	10
Mo nanofilm	0.01 M H_2SO_4	3.09×10^{-11} mol s^{-1} cm^{-2}	0.72	11
MoO_3	0.1 M HCl	29.36 μg h^{-1} $mg^{-1}_{cat.}$	1.9	12
MoS_2/CC	0.1 M HCl	8.48×10^{-11} mol s^{-1} cm^{-2}	0.096	13
Mo_2C nanorod	0.1 M HCl	95.1 μg h^{-1} $mg^{-1}_{cat.}$	8.13	14
Mo_2N	0.1 M HCl	78.4 μg h^{-1} $mg^{-1}_{cat.}$	4.5	15
MoN	0.1 M HCl	3.01×10^{-10} mo1 s^{-1} cm^{-2}	1.15	16
Nitrogen-doped nanoporous graphite carbon membrane	0.1 M HCl	8 μg h^{-1} cm^{-2}	5.2	17
$Bi_4V_2O_{11}/CeO_2$	0.1 M HCl	23.21 μg h^{-1} $mg^{-1}_{cat.}$	10.16	18
VN	0.1 M HCl	8.40×10^{-11} mol s^{-1} cm^{-2}	2.25	19
Nb_2O_5 nanofiber	0.1 M HCl	43.6 μg h^{-1} $mg^{-1}_{cat.}$	9.26	20
$Ti_3C_2T_x$ nanosheet	0.1 M HCl	20.4 μg h^{-1} $mg^{-1}_{cat.}$	9.3	21
d-TiO_2/TM	0.1 M HCl	1.24×10^{-10} mo1 s^{-1} cm^{-2}	9.17	22
B_4C	0.1 M HCl	26.57 μg h^{-1} $mg^{-1}_{cat.}$	15.95	23
Oxygen-doped carbon nanosheet	0.1 M HCl	20.15 μg h^{-1} $mg^{-1}_{cat.}$	4.97	24
Fe_3S_4 nanosheets	0.1 M HCl	75.4 μg h^{-1} $mg^{-1}_{cat.}$	6.45	25

References

1 Y. G. Kresse and J. Furthmuller, *Comp. Mater. Sci.,* 1996, **6**, 15–50.

2 G. Kresse and J. Furthmuller, *Phys. Rev. B,* 1996, **54**, 11169–11186.

3 G. Kresse and J. Hafner, *Phys. Rev. B,* 1994, **49**, 14251–14269.

4 P. E. Blochl, *Phys. Rev. B,* 1994, **50**, 17953–17979.

5 J. P. Perdew, J. A. Chevary, S. H. Vosko, K. A. Jackson, M. R. Pederson, D. J. Singh and C. Fiolhais, *Phys. Rev. B,* 1992, **46**, 6671–6687.

6 H. J. Monkhorst and J. D. Pack, *Phys. Rev. B,* 1976, **13**, 5188–5192.

7 E. Skulason, T. Bligaard, S. Gudmundsdottir, F. Studt, J. Rossmeisl, F. Abild-Pedersen, T. Vegge, H. Jonsson and J. K. Norskov, *Phys. Chem. Chem. Phys.,* 2012, **14**, 1235–1245.

8 L. Zhang, L. Ding, G. Chen, X. Yang and H. Wang, *Angew. Chem., Int. Ed.,* 2019, **58**, 2612–2616.

9 X. Yu, P. Han, Z. Wei, L. Huang, Z. Gu, S. Peng, J. Ma and G. Zheng, *Joule*, 2018, **2**, 1610–1622.

10 Y. Liu, Y. Su, X. Quan, X. Fan, S. Chen, H. Yu, H. Zhao, Y. Zhang and J. Zhao, *ACS Catal.,* 2018, **8**, 1186−1191.

11 D. Yang, T. Chen and Z. Wang, *J. Mater. Chem. A,* 2017, **5**, 18967–18971.

12 J. Han, X. Ji, X. Ren, G. Cui, L. Li, F. Xie, H. Wang, B. Li and X. Sun, *J. Mater. Chem. A,* 2018, **6**, 12974–12977.

13 L. Zhang, X. Ji, X. Ren, Y. Ma, X. Shi, Z. Tian, A. M. Asiri, L. Chen, B. Tang and X. Sun, *Adv. Mater.,* 2018, **30**, 1800191.

14 X. Ren, J. Zhao, Q. Wei, Y. Ma, H. Guo, Q. Liu, Y. Wang, G. Cui, A. M. Asiri, B. Li, B. Tang and X. Sun, *ACS Central Sci.,* 2019, **5**, 116–121.

15 X. Ren, G. Cui, L. Chen, F. Xie, Q. Wei, Z. Tian and X. Sun, *Chem. Commun.,* 2018, **54**, 8474–8477.

16 L. Zhang, X. Ji, X. Ren, Y. Luo, X. Shi, A. M. Asiri, B. Zheng and X. Sun, *ACS Sustainable Chem. Eng.,* 2018, **6**, 9550–9554.

17 H. Wang, L. Wang. Q. Wang, S. Ye, W. Sun. Y. Shao, Z. Jiang, Q. Qiao, Y. Zhu,

P. Song, D. Li, L. He, X. Zhang, J. Yuan, T. Wu and G. A. Ozin, *Angew. Chem., Int. Ed.,* 2018, **57**, 12360–12364.

18 C. Lv, C. Yan, G. Chen, Y. Ding, J. Sun, Y. Zhou and G. Yu, *Angew. Chem., Int. Ed.,* 2018, **57**, 6073–6076.

19 R. Zhang, Y. Zhang, X. Ren, G. Cui, A. M. Asiri, B. Zheng and X. Sun, *ACS Sustainable Chem. Eng.,* 2018, **6**, 9545–9549.

20 J. Han, Z. Liu, Y. Ma, G. Cui, F. Xie, F. Wang, Y. Wu, S. Gao, Y. Xu and X. Sun, *Nano Energy,* 2018, **52**, 264–270.

21 J. Zhao, L. Zhang, X. Xie, X. Li, Y. Ma, Q. Liu, W. Fang, X. Shi, G. Cui and X. Sun, *J. Mater. Chem. A,* 2018, **6**, 24031–24035.

22 L. Yang, T. Wu, R. Zhang, H. Zhou, L. Xia, X. Shi, H. Zheng, Y. Zhang and X. Sun, *Nanoscale,* 2019, **11**, 1555–1562.

23 W. Qiu, X. Xie, J. Qiu, W. Fang, R. Liang, X. Ren, X. Ji, G. Cui, A. M. Asiri, G. Cui, B. Tang and X. Sun, *Nat. Commun.,* 2018, **9**, 3485.

24 H. Huang, L. Xia, R. Cao, Z. Niu, H. Chen, Q. Liu, T. Li, X. Shi, A. M. Asiri and X. Sun, *Chem. Eur. J.,* 2019, **25**, 1914–1917.

25 X. Zhao, X. Lan, D. Yu, H. Fu, Z. Liu and T. Mu, *Chem. Commun.,* 2018, **54**, 13010–13013.